Characterization of MIRCOM, IRSN's new ion microbeam dedicated to targeted irradiation of living biological samples

Francois Vianna-Legros, Geraldine Gonon, Kevin Lalanne, Christelle Adam-Guillermin, Jean Francois Bottollier Depois, Laurent Daudin, Delphine Dugue, Philippe Moretto, Michael Petit, Laurent Serani, et al.

▶ **To cite this version:**

Francois Vianna-Legros, Geraldine Gonon, Kevin Lalanne, Christelle Adam-Guillermin, Jean Francois Bottollier Depois, et al.. Characterization of MIRCOM, IRSN's new ion microbeam dedicated to targeted irradiation of living biological samples. Nuclear Instruments and Methods in Physics Research Section B: Beam Interactions with Materials and Atoms, 2022, 515, pp.20-30. 10.1016/j.nimb.2022.01.007 . hal-03550121

HAL Id: hal-03550121
https://hal.science/hal-03550121

Submitted on 31 Jan 2022

HAL is a multi-disciplinary open access archive for the deposit and dissemination of scientific research documents, whether they are published or not. The documents may come from teaching and research institutions in France or abroad, or from public or private research centers.

L'archive ouverte pluridisciplinaire **HAL**, est destinée au dépôt et à la diffusion de documents scientifiques de niveau recherche, publiés ou non, émanant des établissements d'enseignement et de recherche français ou étrangers, des laboratoires publics ou privés.

Distributed under a Creative Commons Attribution - NonCommercial - NoDerivatives 4.0 International License

Characterization of MIRCOM, IRSN's new ion microbeam dedicated to targeted irradiation of living biological samples

François Vianna[a], Géraldine Gonon[b], Kévin Lalanne[a], Christelle Adam-Guillermin[a], Jean-François Bottollier-Depois[c], Laurent Daudin[d,e], Delphine Dugué[b], Philippe Moretto[d,e], Michaël Petit[a], Laurent Serani[d,e], Jean-Marc Such[a], and Vincent Gressier[a]

a. Institut de Radioprotection et de Sûreté Nucléaire, IRSN, PSE-SANTE/SDOS/LMDN, Cadarache, Saint-Paul-lès-Durance 13115, France
b. Institut de Radioprotection et de Sûreté Nucléaire, IRSN, PSE-SANTE/SERAMED/LRAcc, Fontenay-aux-Roses 92262, France
c. Institut de Radioprotection et de Sûreté Nucléaire, IRSN, PSE-SANTE, Fontenay-aux-Roses 92262, France
d. Université de Bordeaux, Centre d'Études Nucléaires Bordeaux Gradignan (CENBG), Chemin du Solarium, Gradignan 33175, France
e. CNRS, UMR5797, Centre d'Études Nucléaires Bordeaux Gradignan (CENBG), Chemin du Solarium, Gradignan 33175, France

Corresponding author: F. Vianna – francois.vianna-legros@irsn.fr

Abstract

Ion microbeams have emerged as a powerful tool in several domains of radiation biology, from the evaluation of environmental and occupational risks of exposure to low doses of ionizing radiation, to the study of temporal evolution of DNA damage and repair after irradiation of targeted (sub)cellular components. This paper reports the development and commissioning of the IRSN's MIRCOM facility designed for targeted irradiation of living biological samples with a focused ion microbeam extracted in air. This equipment is able to provide protons, alpha particles, and heavier ions such as B, C, O, with energies up to a few MeV. Its performances have been assessed, in a first step, with 4 MeV protons. The beam spot size has been evaluated on CR39 track detectors and living cells at 2.2 ± 0.3 µm, and the targeting accuracy of the system has been measured using online time-lapse imaging at 2.1 ± 0.7 µm.

Keywords: Ion microbeam, radiation biology, time-lapse imaging, targeted irradiation.

1. Introduction

The first micro-irradiation experiments were carried out on biological samples in the 1950's [1]. Since the early 2000's, the scientific community has taken advantage of the many advances in charged particles microbeams to adapt facilities originally dedicated to ion beam analysis to *in vitro* and *in vivo* irradiation. In addition, the development of more and more accurate and user-friendly microscopy technics, linked to the growth of genetic engineering, has given the community innovative and precise tools to study the different radiation-induced mechanisms. Many of these tools can be implemented on microbeam facilities [2].

Conventional radiation sources irradiate the samples as a whole, with a random and statistical distribution of the ionizing particles, which neither makes it possible to ensure that each cell of the

sample has been irradiated in a homogeneous way, nor to target a sub-compartment of the cell. The strength of micro-irradiation studies lies in the ability to deliver a predetermined number of particles of a specific radiation (type and energy) to a whole organism, a tissue, a single cell or a subcellular compartment and with a spatial resolution of the order of a micrometer. The precision of the microbeams therefore makes it possible to control the fraction of cells crossed by the particles, the number of particle(s) for each target, and the location of the particle track at the cellular or subcellular level.

The microbeam approach is of particular importance in mechanistic studies related to the risks associated with exposure to low doses/fluences of charged particles. This is because it is now possible to determine the actions of strictly single particle tracks and thereby mimic, under *in vitro* conditions, exposures at low radiation dose that are significant for protection levels, especially those involving medium- to high-LET (Linear Energy Transfer) radiations. Overall, microbeam methods provide a new dimension in exploring mechanisms of radiation effects at the cellular level.

Using ion microbeams, experiments have shown that even a single alpha particle traversal can have toxic and mutagenic effects [3,4]. Several experiments have also shown that biological responses are not always linear at low fluences, since hypersensitivity [5], bystander effect [6–9], and genomic instability [10,11] may increase the risk, whereas adaptive response [12] may act as a protective mechanism.

By allowing the targeting of nuclear DNA, microbeams have also been used to probe the spatial and temporal evolution of DNA damage and repair, leading to the development of potential clinical and gene therapy targets that may be used, for example, for hereditary disorders and cancers [13].

Another advantage of microbeams is that it enables to target other subcellular components than the nucleus, allowing to go beyond studies of direct DNA damage–mediated effects. Indeed, it has been traditionally accepted that the biological effects of radiation exposure were only the consequence of DNA damage in cells whose nuclei were targeted by radiation. However several groups have shown that micro-irradiation of cytoplasm can also lead to biological effects [14,15]. Importantly, increased levels of mutations were found after cytoplasmic irradiation using alpha particles, with potentially more harmful consequences due to the low cell killing, than after nuclear traversals [16]. Moreover, by using a mitochondrial DNA depleted cell, it was demonstrated that mitochondria play an essential role in cytoplasmic radiation induced genotoxic damage in mammalian cells [17].

One of the major scientific challenges in radiation biology is to fill the knowledge gap still existing between the physics of ionizing radiation and the first events induced at the cellular and tissue scale. It contributes to supporting the new paradigms of radiobiology which, contrary to the historical dogma of the "target cell" and DNA damage by itself, would favor inter and intra-cellular communications in the genesis of long-term radio-induced responses. A microbeam constitutes an essential tool aimed in particular at better identifying and preventing the side effects resulting from the use of ionizing radiation for therapeutic purposes and those aiming at a better understanding of the effects of low doses/fluences.

Extending the application on *in vitro* cell micro-irradiation, developments have been made to take into account the complex responses at the tissue level using 3D culture methods [2,13]. DNA double-strand break formation has been for example studied in directly irradiated or bystander cells in 3D artificial tissue systems [18] but also *in vivo* in intact living mammal [19]. Additionally, to gain further insights into spatial and temporal biological responses in micro-irradiated cells, and link cellular to functional biological levels, the use of small animal models such as nematodes [20,21], silk worms [22] and fish embryos [23] has been developed.

In the framework of its mission to improve knowledge on the effects of ionizing radiation on human health and environment, the Institute for Radiological Protection and Nuclear Safety (IRSN, France) has decided to implement an ion microbeam set-up, open to the scientific community, dedicated to these studies. This facility is called MIRCOM (Ion microbeam for radiation biology at the cellular and multicellular scales), and is designed to perform targeted micro-irradiation of living biological samples and to follow the radiation-induced effects both online and offline. The first irradiation of biological samples has been carried out at the end of 2018.

After the description of the whole facility and of the microbeam itself, this paper presents the method used to characterize the MIRCOM microbeam, and the first 4 MeV proton beam performances.

2. Description of the MIRCOM facility

The MIRCOM facility is located at Cadarache research center (Saint-Paul-lez-Durance, France), and is operated by the micro-irradiation, neutron metrology and dosimetry laboratory (LMDN) from the Health and Environment Division of IRSN. This facility is constituted by a beamline designed to deliver ion microbeams to perform targeted micro-irradiation of living biological samples, with a controlled number of ions of a given energy. It is linked to the AMANDE (Accelerator for neutron metrology and applications in external dosimetry) facility, which is the French reference for neutron metrology in monoenergetic fields since 2005 [24,25].

The MIRCOM facility has specifically been conceived to carry out radiation biology experiments, the main illustration being the fully equipped biology laboratory, located next to the microbeam irradiation room. It is used to prepare biological samples for irradiation, and to quickly perform offline post-irradiation analysis, in addition to online time-lapse imaging. With a surface of 80 m^2, it is mainly composed of two cell culture rooms designed to prevent any risk of contamination of the samples or dissemination in the environment. It has all the necessary equipment to perform cell culture, genetic engineering, immunostaining, etc. It is also equipped for time-lapse imaging, with an AxioObserver™ Z1 inverted epi-fluorescence microscope, coupled with an Apotome.2™ (Carl Zeiss Microscopy GmbH, Germany) and an incubation chamber (temperature and CO2 regulation), for long-term image acquisition of living samples.

2.1. Particle accelerator

AMANDE and MIRCOM facilities share the same ion sources and particle accelerator.

Three negative ion sources are available to produce ions in MIRCOM: two “multicusp” ion sources delivering protons, deuterons (not used in MIRCOM) and helium ions [26], as well as a cesium sputtering ion source [27,28] producing heavier ions such as C, B, O, etc. The ions are then accelerated by a 2 MV Tandetron™ particle accelerator. The ion sources and this electrostatic accelerator have been manufactured by the High Voltage Engineering Europa B.V. company (HVE, Netherlands) [29]. This type of accelerator is used on several facilities around the world and has shown to be well suited for microbeam applications because of its ability to produce continuous ion beams with relatively good brightness and stability [30–35]. In addition, a Tandetron™ particle accelerator provides a better versatility in terms of ion type production capabilities than single-ended machines because the ion sources are located outside the accelerator. The accelerated ions reach energies depending on the accelerator high voltage (0.05 to 2.0 MV) and their charge state.

2.2. Energy calibration

Two 90° electromagnetic dipoles are present in the beamline after the accelerator. The first one is used to select the ions according to their energy, charge state and atomic mass and then inject the selected

ions into the microbeam line. When this so-called "MIRCOM 90° magnet" is switched off, the ion beam goes into the AMANDE beamline for monoenergetic neutron production. The other 90° dipole is located downstream the microbeam 90° magnet and selects the ions sent on AMANDE beamline. The magnetic field in this "AMANDE 90° magnet" is stabilized using a nuclear magnetic resonance teslameter and associated gauss probes, with a feedback loop on the magnet power supply. The relation between the magnetic field and the ion beam energy is calibrated using standard nuclear reactions. Through this method, the ion beam energy can be defined with a relative uncertainty lower than $5x10^{-4}$ [25,29].

To obtain a beam of a given energy, the ions are first sent through the "AMANDE 90° magnet", and the terminal voltage of the accelerator is adjusted to its correct value, using the energy calibration of the magnet. Then, the terminal voltage value is fixed and the "MIRCOM 90° magnet" is switched on. Its magnetic field is adjusted so that the ion beam is sent into the microbeam line through the different collimators and apertures. The stability of the beam is ensured by two pairs of slits, located before and after the magnet, that are used to maintain a correct beam trajectory inside the magnet by using feedback loops.

2.3. Microbeam line

MIRCOM's microbeam line is a horizontal beamline based on focused ion beam technics. It has been designed and built by CENBG (Bordeaux-Gradignan center for nuclear studies, Bordeaux University – CNRS/IN2P3, France), based on its existing microbeam line, described in [36]. Its general principle is shown on Figure 1.

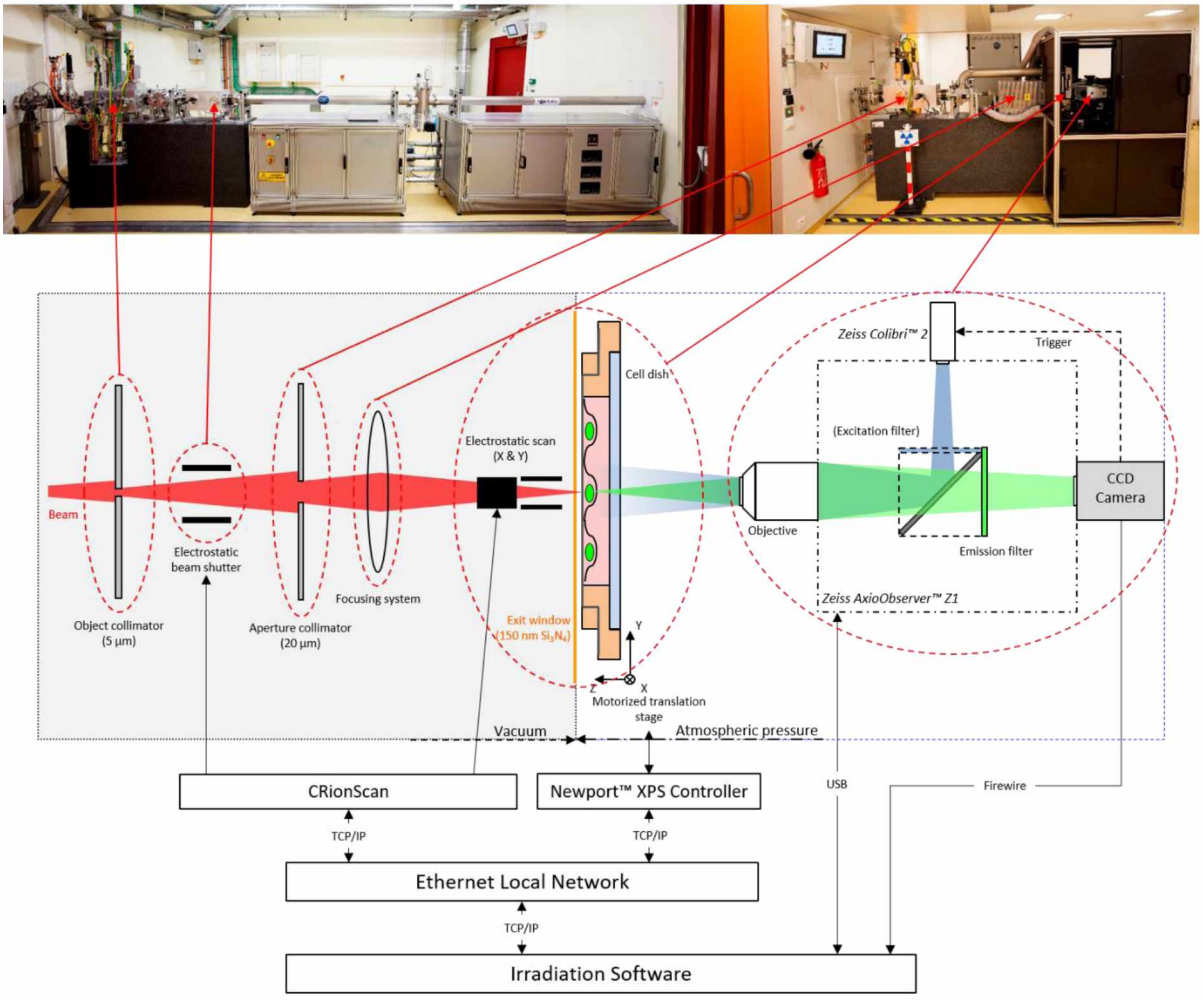

Figure 1: Overview of the microbeam line of the MIRCOM facility. The top image is a panoramic view of the MIRCOM microbeam line. The ion beam propagates from the left to the right of the image. The beamline is 10 m long. The bottom part of the figure is adapted from [36]*. It describes the general principle of the beamline. The ion beam is collimated and focused down to a sub-micrometer spot, before in-air extraction through a 150 nm thick Si_3N_4 window. The cell dish is positioned vertically in front of the vacuum window on a motorized translation stage. A microscope is used to locate and target the cells and to perform online time-lapse imaging. The end-station is located inside a thermo-regulated dark chamber to keep the samples at 37°C. The location of the beamline main components on the top image is given by the red arrows.*

The ion beam enters the beamline though two successive stages of horizontal and vertical slits, and an "object" aperture of typically 5 µm in diameter. Most of the beam coming from the accelerator is stopped by these water-cooled slits to protect the well-defined pinhole object aperture from radiation and heat damage. Only ions passing through this "object" are focused, a few meters downstream, by four magnetic quadrupoles (OM-50™ quadrupoles, Oxford Microbeams Ltd., United Kingdom), described in [37], associated in a "Russian quadruplet" configuration. This quadruplet guarantees a high and identical demagnification factor on both horizontal and vertical planes.

This system has been designed to achieve a demagnification factor of 14, resulting in a theoretical beam spot size of 0.36 µm in vacuum (image size) for a 5 µm object aperture. A second aperture stage located upstream the focusing system is coupled with the first aperture to act as a collimator: its role is to eliminate the ions scattered too far from the optical axis, thus reducing optical aberrations. This second aperture is also used to reduce the ion rate on the target down to a few thousand ions per second.

The beam then reaches the extraction window. To maintain the 1 bar differential pressure between the vacuum of the beamline (10^{-7} to 10^{-8} mbar), and the air pressure in which the samples are located, a very thin Si_3N_4 membrane (150 nm thick, 1 x 1 mm^2, Silson Ltd, U.K.) is used. It is thin and light enough to let MeV ions to pass through with a very small energy loss and acceptable scattering. A dedicated vacuum system, controlled by an Industrial Siemens S7-1500 PLC (Programmable Logic Controller) is securing the pumps in case of a window breakdown.

Just before the extraction, electrostatic scanning plates are used to rapidly and precisely move the ion beam to the requested irradiation position of the target (X and Y axes). The beam can be scanned on the sample over a 700 x 700 μm^2 surface for 4 MeV protons, and can be moved from one point to another in less than 10 µs. As it is based on electrostatic deflection of ions, the scanning limitations are ion charge and energy dependent. To achieve such scanning performances, Matsusada high-speed and high-voltage amplifiers (+/-1kV – Model AS-1B3) are used to apply opposite voltages on each pair of deflection plates. With this equipment, precise and fast targeted irradiations can be achieved.

A fast beam shutter is located upstream, just after the object aperture. It has been designed to control the irradiation by quickly shutting it down as soon as a predefined time (from 10 µs up to 10 s) or a number of particles has been reached on the targeted position. This shutter is an electrostatic beam gate made of a pair of deflection plates coupled with a very fast high voltage pulse generator (DEI PVM-4210), delivering an 1800 V electrical field in 20 ns.

The beam control (opening, scanning) and the ion counting are managed by a dedicated system (called ''CRionScan'') consisting of a stand-alone real-time scanning and imaging instrument based on a Compact Reconfigurable Input/Output (Compact RIO) device from National Instruments™ [38]. The CRionScan is remotely controlled by a custom-made irradiation software via a local Ethernet network, as illustrated by Figure 1.

2.4. End-station

The design of the microbeam end-station is based on the CENBG one, described in [36]. The main equipment of this end-station is the AxioObserver™ Z1 inverted epi-fluorescence microscope (Carl Zeiss Microscopy GmbH, Germany). The samples are installed and maintained vertically to be irradiated by the horizontal focused ion beam. For this reason, the microscope has been customized so that its objectives can face the extraction window of the microbeam. The light source used for fluorescence is a LED-based Colibri.2™ (Carl Zeiss Microscopy GmbH, Germany). Sample visualization is carried out by a monochromatic AxioCam™ MRm rev. 3 CCD camera (Carl Zeiss Microscopy GmbH, Germany). It is used to locate the regions of interest in a culture dish, select and place the samples to irradiate in the microbeam axis, as well as perform online time-lapse imaging, using single- or multi-fluorescence. Each microscope parameter (objective wheel, focus, fluorescence mode, image acquisition ...) can be remote-controlled by the irradiation control software, developed by CENBG.

The culture dish is placed between the microscope and the beam exit window on a sample holder. This sample holder is mounted on a 3 axes high precision motorized stage (Newport™ M436 linear stages moved by Newport™ LTA- HS actuators). The stages movement range of 5 cm in X and Y directions (perpendicular to the beam axis) allows the exploration of the whole culture dish. The Z axis is used to bring the cell dish as close as possible to the exit window, i.e. approximately 250 µm due to the geometry of the system and the relative fragility of the window.

The dish itself is described in [36]. It has been designed to perform cell culture directly inside it, while minimizing optical distortions to optimize the targeting accuracy. A 4 µm-thick polypropylene foil

(Goodfellow), on which cells will be cultured, is stretched on a rigid body made in PEEK (Polyether ether ketone) and clipped in place, avoiding thus the use of any glue.

The whole end-station is placed inside a dark incubation cage, so that the sample is maintained in a temperature-controlled atmosphere. This is particularly useful for long-term time-lapse imaging (up to a few hours).

Before reaching the sample, the beam goes through the 150 nm thick Si_3N_4 extraction window, the 250 µm thick residual layer of air, and the 4 µm thick polypropylene foil. The ion scattering in these different layers leads to an energy loss and a degradation of the focused beam lateral resolution. This has to be taken into account when evaluating the energy deposition during the irradiation. The resulting energies, LETs and projected ranges in water, calculated with SRIM [39], are given in Table 1 and the LETs are represented in Figure 2. The large variety of ions and energies allow the exploration of a wide range of LETs.

Table 1: Energies at the sample position for the ions available on MIRCOM, and their associated LET and projected range in water. LETs and projected ranges were calculated with SRIM [39] *using the geometry described in chapter 2.4. Minimal energies were defined to allow a range in water of a few µm.*

Ion type	Energy in vacuum (MeV)	Energy at the sample position (MeV)	LET in water (keV·µm^{-1})	Projected range in water (µm)
H	0.5 to 4.0	0.3 to 4.0	10 to 51	5 to 241
He	1.5 to 6.0	0.5 to 5.6	80 to 221	4 to 44
B	4.0 to 12.0	0.9 to 9.2	422 to 704	4 to 16
C	5.0 to 12.0	1.1 to 8.2	527 to 887	4 to 12
O	6.4 to 12.0	1.2 to 6.0	585 to 1254	3 to 8

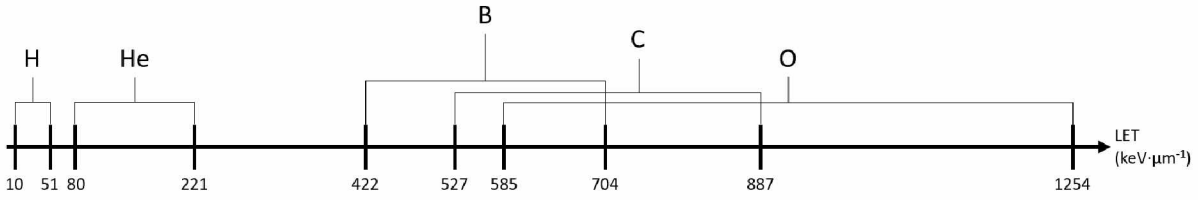

Figure 2: LET in water at the sample position for the ions and energies available on MIRCOM, calculated using SRIM [39].

3. Beam monitoring

In order to control, as accurately as possible, the deposited energy inside the target, a precise monitoring of the number of ions sent on target is mandatory. This can be performed by two methods, i.e. either controlling the opening time of the beam, or using an ion detector that has to be placed before the sample, since the ions do not have enough energy to go through the dish. The first method has the advantage of avoiding any additional materials on the beam path, thus maintaining optimal beam conditions. However, it increases the uncertainty on the number of ions, which follows a Poisson law, and requires a very good stability of the beam intensity. To ensure this, the emission rate of the microbeam has to be controlled regularly. The second method allows a precise on-line counting of the ions, down to one ion per irradiation point, and reduces greatly the uncertainty on the number of hitting ions. However, putting the detector before the sample introduces new uncertainties on the energy and position of the ions due to the induced straggling.

At this time, only the first monitoring method (control of the beam opening time) is used at MIRCOM facility. It will be progressively completed through several upgrades, with different kinds of ion detectors.

3.1. Materials and Methods

The monitoring of the beam emission rate in air is carried out with a PIPS (Passivated Implanted Planar Silicon) detector (PD50-12-100AM, Mirion Technologies, France). The detector is mounted on the end-station microscope, on the objective wheel, and can thus easily be placed in front of the beam exit window to perform the ion counting in the absence of a culture dish. The thickness of the sensitive layer of this detector is 100 µm which is sufficient to collect enough energy to generate a reliable counting signal. This detector can then be considered to have an efficiency of 100% and constitutes the reference. The PIPS signal is amplified by a Canberra 2004 charge sensitive preamplifier and then discriminated by an ORTEC 590A Timing Single Channel Analyzer (TSCA). The SCA output is directly connected to one of the CRionScan counting input. The count rate can then be visualized on the CRionScan webpage [38] and each measurement can be recorded by the irradiation software. Sets of single measurements can then be automatically performed, so that a reliable mean emission rate value can be obtained.

Measurements are first carried out at the end of the tuning phase and, then, regularly to monitor the stability of the beam current throughout the experiment. A beam current of a few thousand ions per second is typically used for 4 MeV protons. An example of a set of measurements, for an opening time of 100 ms, is shown on Figure 3: the mean number of ions over 961 measurements is of 194 with a standard deviation of the Gaussian fit of σ = 15, close to the expected value (14) from a Poisson law.

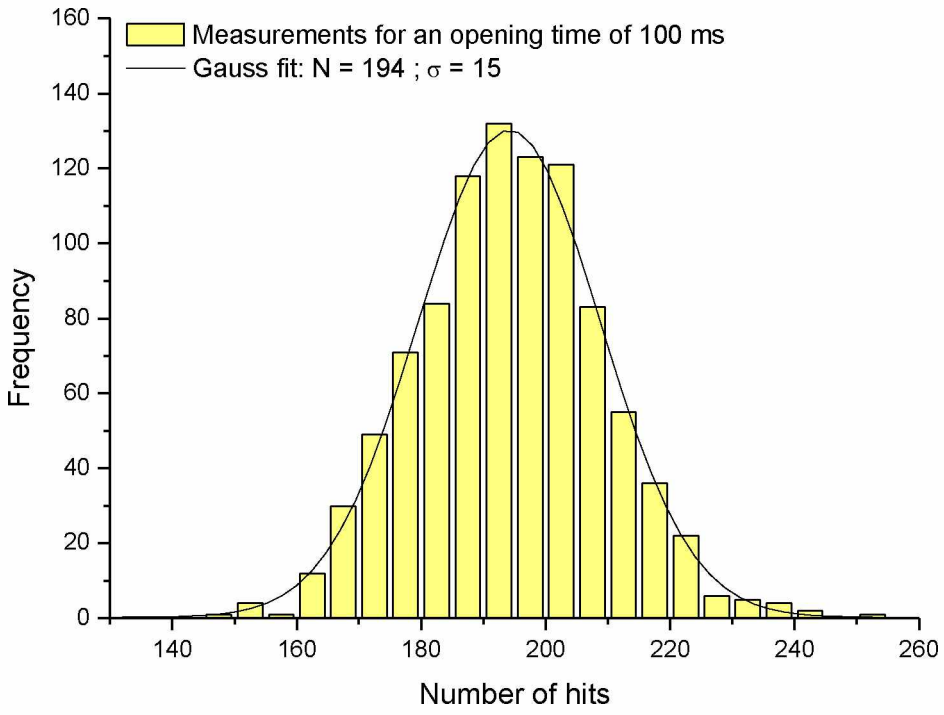

Figure 3: Example of the distribution of the number of hits, used to monitor the mean counting rate of the microbeam between each irradiation. 961 measurements with a beam opening time of 100 ms were performed in this case, which resulted in a mean number of ions N = 194, with a standard deviation σ = 15. The relative fluctuation is 8%.

3.2. Results

Figure 4 shows the evolution over time of the mean counting rate on the PIPS detector for 4 MeV protons. It is representative of a typical behavior of the microbeam for protons. This behavior of the beam can be divided in two phases. First, a "warm-up" phase, during which the different elements of the beamline (ion source, particle accelerator, bending magnets ...) are still stabilizing. This results in a rather unstable beam current during about an hour. Then, the beam enters a nominal phase, in which

the beam current stays stable, as illustrated in Figure 4. Nevertheless, to ensure that the beam does not undergo major fluctuations during irradiations, the mean counting rate in the PIPS is measured between each sample. No significant variation of the beam was observed between two consecutive controls during a period of 4 hours.

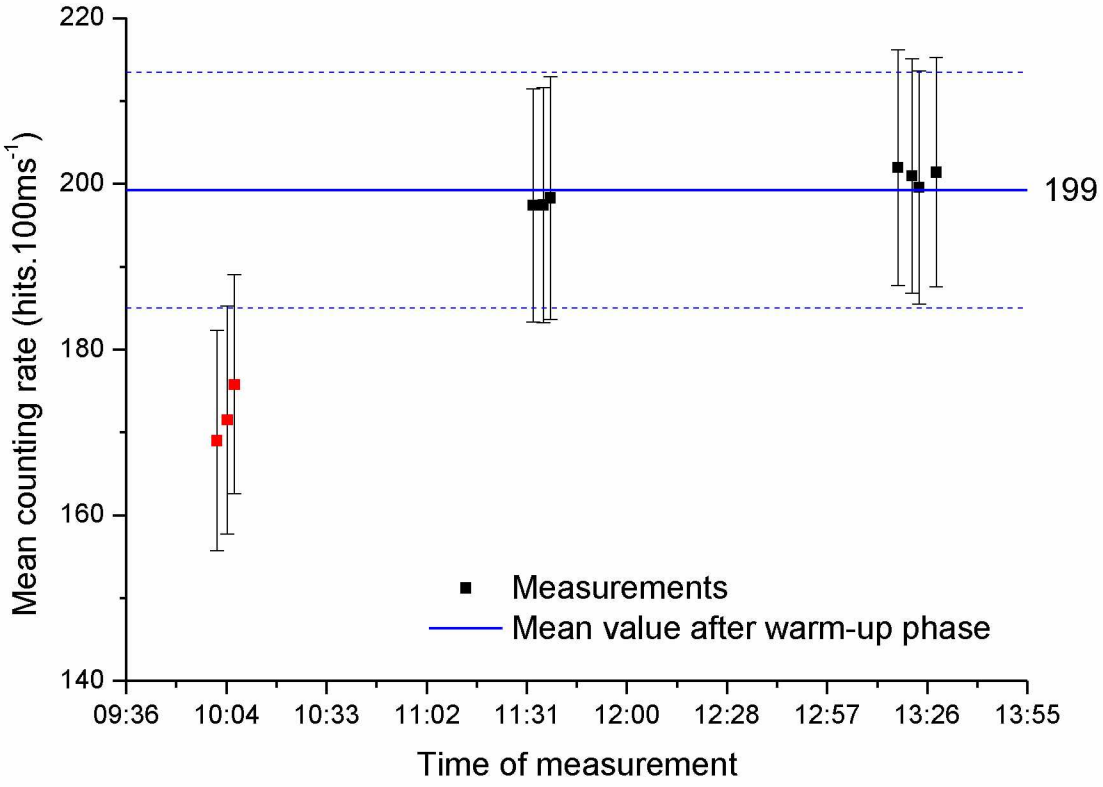

Figure 4: Evolution over time of the mean counting rate on the PIPS detector for 4 MeV protons. Each point represents the mean value for 1024 measurements of 100 ms. The error bars represent the statistical distribution of these measurements, with a confidence interval of 68% (k=1). The red dots correspond to measurements made during the "warm-up" phase of the system, where the counting rate slowly increases to reach its final value. After this phase, the ion emission becomes stable, as illustrated by the black points. The blue lines represent the statistical distribution of the measurements after the "warm-up" phase (k = 1).

4. Beam characterization

The main goal of the MIRCOM facility is to target cellular, sub-cellular, or even sub-nuclear components of living biological samples. In that aim, both the spatial resolution and the targeting accuracy of the focused ion beam needs to be in the micrometer range. The control of these performances is therefore a prerequisite to the use of the microbeam.

The beam spot size can be calculated using numerical modelling methods based on Monte-Carlo codes such as SRIM [39] or Geant4 [40]. Taking into account the different layers of matter crossed by the ion beam before reaching the samples, a theoretical beam diameter of 1.9 µm has been calculated using SRIM. Nevertheless, to fully assess the performances of MIRCOM's microbeam, an experimental determination is required.

The first step consisted of CR39 track detectors irradiations. The use of this technique allows a visualization of the ions' tracks and is commonly used to evaluate the performances of microbeams [34,36,41–44]. However, a direct transposition of the results obtained on track detectors to assess the performances of the microbeam on cells is not ideal, as differences in the irradiation setup can affect

the beam geometry. A confirmation of these results on living samples is needed to have a characterization of the ion beam in "routine" conditions.

4.1. Materials and Methods

4.1.1. Track detector irradiation

The scanning abilities of the microbeam and the beam spot size have been evaluated with irradiations of CR39 track detectors (TASTRAK PADC, Track Analysis Systems Ltd., U.K.). By irradiating the track detectors according to different geometrical patterns, it is possible to verify that the ion beam is not influenced by the type or size of the used pattern. The beam spot size can be evaluated by measuring the diameter of the impact on CR39 that underwent the same etching protocol.

Three track detectors were successively placed at the sample position of the microbeam and exposed to 4 MeV protons according to different patterns: a network of cross patterns of 5 points, with spacing ranging from 5 to 25 µm between each point, as well as a network of single points, with spacing ranging from 5 to 50 µm between each point. Irradiations were carried out with 10 and 100 protons per point. The CR39 were then chemically etched with potassium hydroxide (KOH, 12 $mol \cdot L^{-1}$) at 80°C for 15 minutes. Imaging was performed in phase contrast, on a Zeiss AxioObserver™ Z1 inverted microscope, using a 20X objective (Zeiss LD Plan-NEOFLUAR 20x/0.4 Ph2 Korr). Image processing was performed using the Zen imaging software from Zeiss.

4.1.2. Cell irradiation

To estimate the beam spot size, and to measure the targeting accuracy of the microbeam, the use of time-lapse imaging of fluorescent cells is a fast and reliable method to visualize directly the early consequences of the microbeam irradiation [36,45]. The major direct consequences of exposing cell nuclei to ionizing radiation are DNA single- and double-strand breaks (SSBs and DSBs, respectively). DNA damage-sensing and repair proteins can act by re-locating to the site of DNA damage or by being subjected to post-translational modifications directly on sites. Among them, the X-ray repair cross-complementing group 1 (XRCC1) protein is a scaffold involved in the overlapping of single strand break repair (SSBR) and base excision repair (BER) pathways [46,47] and participates in other repair pathways as well [48]. Consistent with its DNA repair functions, XRCC1 has primarily nuclear localization [49] and is known to accumulate within a few tens of seconds at damaged sites [50].

For the characterization of the microbeam, the relocalization of the fusion protein XRCC1-GFP, composed of the XRCC1 protein fused with the green fluorescent protein (GFP), was studied, using the method described in [36].

Osteoblast-like cells U2OS (ATCC® HTB96™) obtained from LGC Standards (Teddington, Middlesex, U.K.) were cultured in Dulbecco's modified Eagle's Medium (DMEM) containing 10% fetal bovine serum (FBS) and supplemented with 10 U/mL penicillin and 100 $\mu g \cdot mL^{-1}$ streptomycin (15140122, Life Technologies). They were maintained in 37°C humidified incubators with an atmosphere of 5% CO_2 (vol/vol) in air. Approximately 48 h before irradiation, confluent cell cultures were trypsinized and cells were plated at 50% confluence into the cell dishes described in section 2.4. The polypropylene foil surface was pretreated with CellTak (Corning) at 2 $\mu g \cdot cm^{-2}$ in order to facilitate cell attachment. Twenty-four hours before irradiation, cells at 70-80% confluence were transiently transfected with a plasmid harboring XRCC1-GFP (Origene, ref. RG204952) using the Lipofectamine 3000 reagent from Life technologies (Carlsbad, CA, USA) according to manufacturer's protocols.

Just before irradiation, cell dishes were sealed with a cover glass and placed in a specific dish holder, which was positioned perpendicularly to the beam in front of the exit window. It was then brought closer to the Si_3N_4 window, down to a distance of ~250 µm.

To assess the characteristics of the microbeam, cells were irradiated with 4 MeV protons according to a cross pattern of 5 points. Each point is separated from its neighbor by 4 µm and exposed to 1000 ± 32 protons. Imaging of the XRCC1-GFP cells was performed with a 20X objective (Zeiss LD Plan-NEOFLUAR 20x/0.4 Korr) and automatic shape recognition was performed to select the relevant nuclei.

Time-lapse imaging was performed online, directly by the irradiation software that can control camera exposure time, interval between images, total length of the acquisition, and fluorescence modes. To avoid unnecessary photobleaching, the Zeiss Colibri2™ fluorescence light source was controlled by the camera trigger and was only switched on during the image acquisition (typically a few hundred milliseconds for each image). Cells were kept in the microbeam chamber less than 30 min.

Image processing and analysis were then performed using the Fiji software [51]. 163 nuclei in 2 different cell dishes were irradiated and analyzed.

4.2. Results

4.2.1. CR39 track detector irradiation

Figure 5 shows an example of a CR39 track detector after irradiation with 4 MeV protons and chemical etching. The different patterns are easily visible and show that the requested type of pattern and spacing have been respected, validating the beam scanning system. It should be noted that the quality of the microscope system, coupled with the phase contrast technic, allows to visualize zones irradiated with a rather small number of protons (down to 10). The difference between the points irradiated with 10 protons and those irradiated with 100 protons, which have sustained more damages, is also clearly visible. All points underwent the same chemical etching, so the more damaged a point has been, the bigger it appears, even though the ion beam itself is the same size. For this reason, the evaluation of the beam spot size is determined by measuring the diameter of the impacts induced by the lower number of protons, i.e. 10 protons.

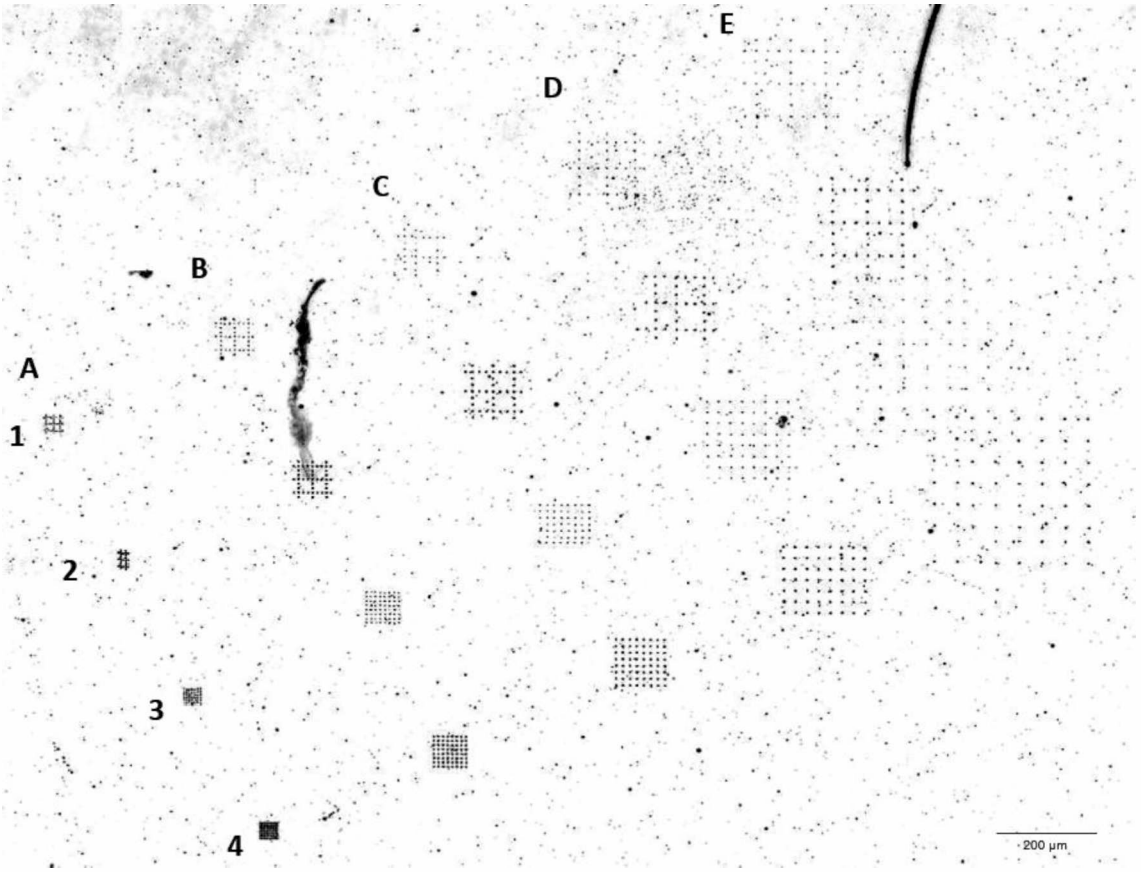

Figure 5: Negative image of a CR39 track detector after irradiation with 4 MeV protons and chemical etching. The impact points are visible as the black dots that follow a cross (rows 1 and 2) or square (rows 3 and 4) pattern. Rows 1 and 3 were irradiated with 10 protons per point. Rows 2 and 4 were irradiated with 100 protons per point. The patterns and difference of number of protons per point are visible on this image. Individual dots outside the patterns are background noise inherent to the track detector and the imaging technique.

Impact diameters were measured and compared for each type of pattern and each spacing. The relative standard deviation on all the measured values is of 15%. Considering the effect of the chemical etching and the possible distortions induced by the imaging technique, this does not reveal significant difference of the impact diameter on the different patterns and CR39 samples or substantial influence of the beam scanning system on the beam shape itself.

The mean impact diameter, as calculated from three CR39 track detectors irradiated with 10 protons of 4 MeV energy with MIRCOM, is 3.4 ± 0.6 µm (k = 1). Considering the chemical etching of the induced damages on the CR39, this beam spot is expected to be overestimated.

4.2.2. Cell irradiation

Figure 6 shows an example of the real-time accrual of the XRCC1-GFP fusion protein to the site of induced DNA damage in a U2OS cell nucleus after 4 MeV protons exposure. It illustrates the capability of the microbeam to select, target and irradiate specific sub-cellular and even sub-nuclear areas of living biological samples, as well as to visualize online the effect of this irradiation after only a few seconds. This opens up ways to characterize fast radiation-induced phenomena and allows the user to rapidly assess microbeam characteristics such as the beam spot size and the targeting accuracy of the system.

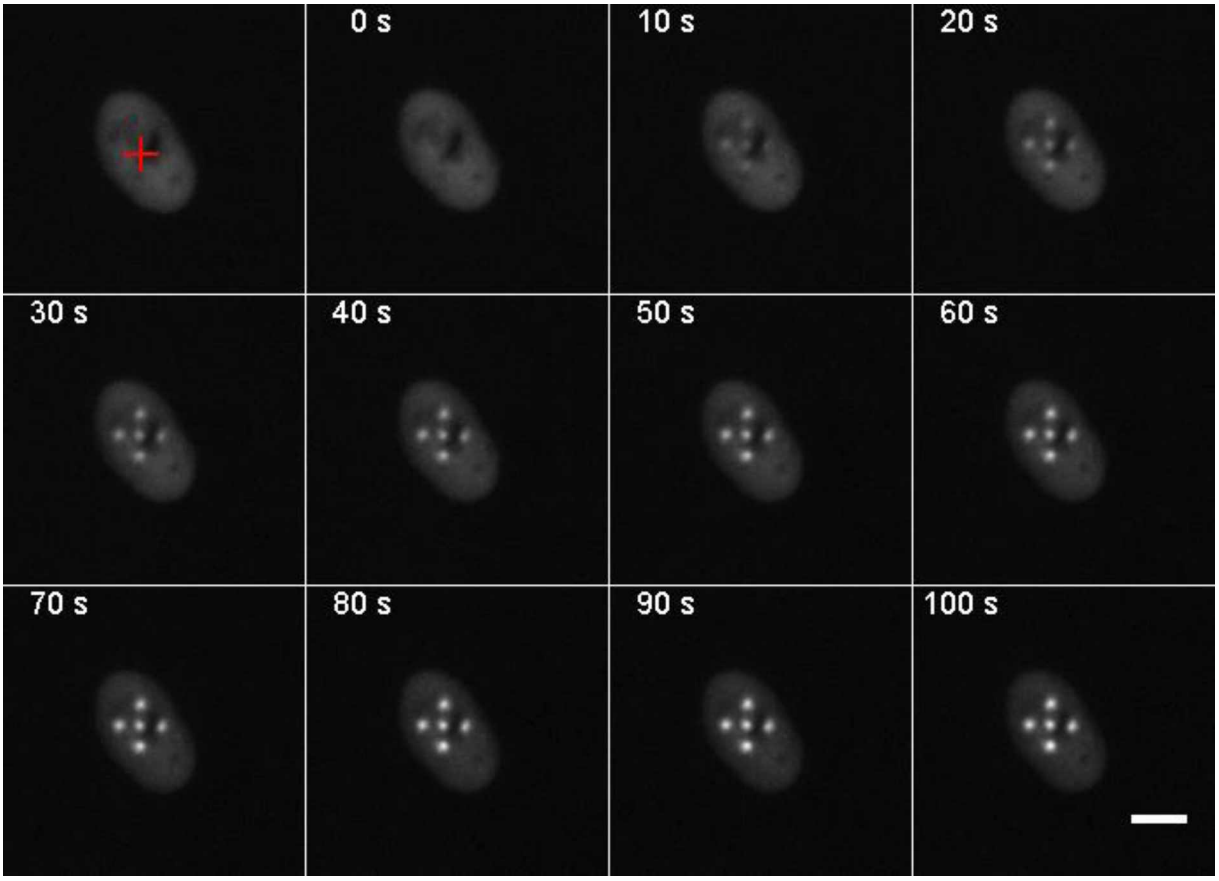

Figure 6: Real-time accumulation of the XRCC1-GFP protein in a U2OS cell nucleus after irradiation with 4 MeV protons. The nucleus was targeted in the center (red cross) and irradiated according to an 8 µm-wide cross pattern of 5 points. Each point has been irradiated with 1000 ± 32 protons. The irradiation starts at 0 s. Scale bar: 10 µm.

The beam spot size can be evaluated by measuring the diameter of the damaged areas on the irradiated nuclei. For 4 MeV protons, the mean beam spot size, measured on 163 irradiated nuclei in 2 different cell dishes, is of 2.2 ± 0.3 µm (k = 1), i.e. smaller, as expected, than the value determined with the CR39 and in agreement with the value obtained by simulation. However, this determination is, as for CR39, a visualization of the consequence of the irradiation and not a direct measurement of the beam itself. A small overestimation is therefore awaited due to the diffusion of the fluorescence light in the different elements between the cell and the camera (culture medium, air, objective …). For this reason, the beam spot size is considered to be slightly smaller than the size of the damaged areas on cells.

The targeting accuracy is determined by measuring the distance between the targeted point (red cross on Figure 6) and the center of the irradiated zone. Figure 7 shows the evolution of the targeting accuracy on different microscope fields of one cell dish. The size of a microscope field acquired with a 20X objective is 430x322 µm. Each analyzed field is distant from its neighbor by at least 1 mm, to cover a large area of the cell dish. A good reproducibility is obtained, whatever the position of the selected area of interest in the culture dish is. By performing the same measurements on 163 irradiated nuclei in 2 different cell dishes, the determined targeting accuracy value is 2.1 ± 0.7 µm.

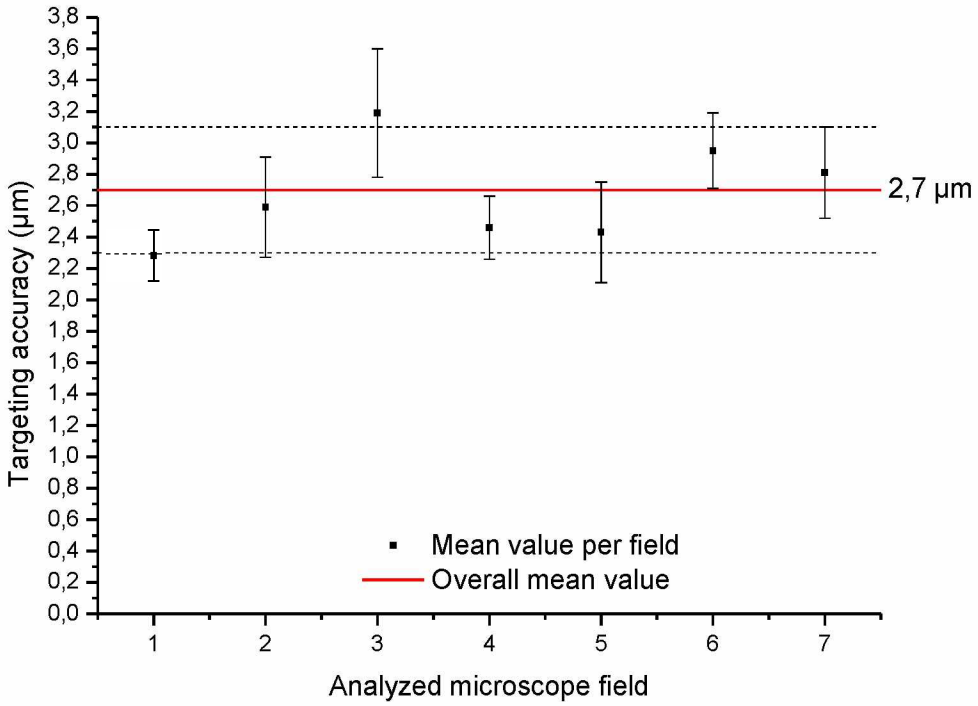

Figure 7: Evolution of the targeting accuracy on different microscope fields of one cell dish. The error bars represent the statistical distribution of the targeting accuracy for each field, with a confidence interval of 68% (k=1).

5. Discussion and future work

The results reported in this paper are in good agreement with the technical specifications of MIRCOM and illustrate the general validation method that will be applied to characterize the microbeam performances for the other available ions in the near future.

First, the study of the beam stability over time allows to verify the quality of the beam tuning (some instabilities can come from an incorrect tuning) and to control the number of ions sent on target by selecting an appropriate beam opening time.

Both aspects have been validated by the results described here for 4 MeV protons. Figure 3 illustrates the fact that the number of particles on each target follows a Poisson law, with a mean number of ions N and a standard deviation $\sigma = \sqrt{N}$. In addition, the good beam stability over a long period of time (Figure 4), associated with a regular monitoring of the counting rate in the PIPS detector, make the opening time as a reliable beam monitoring method for protons at MIRCOM facility. For the other available ion types, a similar study is in progress. Preliminary results for alpha particles show a comparable behavior but with a slightly lower beam current stability, requiring more control measurements of the counting rate in the PIPS detector.

However, this method is only valid if the mean number of ions requested is not too small due to the $1/\sqrt{N}$ relative uncertainty on the number of ions (3%, 10%, 30% for respectively 1000, 100 and 10 ions). The worst case occurs if only 1 ion is requested. Following the Poisson law with parameter λ = 1, the probability to be in this case will be only 37%, whereas 37% of the irradiation will have no ions, and 26% will have 2 or more ions. If the precision of the number of particles on each target is an important parameter for the irradiation, the only way to ensure an acceptable uncertainty with a limited number of ions is then to use particle detectors. These detectors need to have a detection efficiency as close as possible to 100% and have to be thin enough to limit the energy degradation and the straggling of the focused ion beam. Two types of detectors are currently being implemented on MIRCOM. For

protons, thin single crystal diamond membranes, similar to those developed by CENBG and the Diamond Sensors Laboratory from CEA-LIST (Gif-sur-Yvette, France) [52] will be used. A first version of this detection method will be implemented on the beamline by the end of 2022. Alpha particles and heavier ion counting will rely on the detection of secondary electrons ripped from the extraction window when the ions go through and amplified by a channel electron multiplier [53]. This detection method will be available by mid-2022.

The beam geometry is an essential information. Indeed, knowing the performances in terms of beam diameter and targeting accuracy can help defining and validating the irradiations as well as the different experimental setups that can be performed. Moreover, in order to compare experimental data with simulation of the irradiation using numerical tools such as Geant4, an accurate knowledge of the beam geometry at the targets is required.

Following the measurements of the irradiation consequences, both on CR39 solid track detectors and living cells, an estimation of the focused beam spot size for 4 MeV protons has been carried out leading to an upper value of 2.2 ± 0.3 µm. This value is coherent with what was expected, from numerical simulations, and is comparable to what has been measured at other facilities having the same focusing systems and end-station geometries [34,36,42,54–56]. However, only indirect methods were used for this estimation. For measurements on CR39, the chemical etching induces an overestimation of the actual beam diameter of a few micrometers. This overestimation is reduced by determining the size of the damaged areas on living cells following the irradiation, but still remains due to the possible diffusion of the fluorescence light in the medium and the optical elements of the microscope. Although it can be simulated using Monte-Carlo codes such as SRIM or Geant4 [36,57,58], it would be interesting to implement a more direct method to measure the beam geometry in air. Fibered nanosensors are being developed by the PIV (Physics and Engineering for Living Systems) department of CINaM (Interdisciplinary Center of Nanoscience of Marseille, France), and are currently being adapted on the MIRCOM microbeam for this purpose. The active part of these sensors is integrated at the tip of a pulled optical fiber. High sensitivity and lateral resolution (20 nm demonstrated) are expected and will allow a precise measurement of the lateral resolution of the microbeam [59].

The measured targeting accuracy of the MIRCOM microbeam is of 2.1 ± 0.7 µm for 4 MeV protons. This value is comparable to similar facilities, in particular the CENBG microbeam on which IRSN microbeam design was based [34,36,42,54–56]. Associated with a good lateral resolution of the focused ion beam, it allows a precise, reliable and reproducible targeting of micrometric structures of the samples, either nuclear/sub-nuclear structures (hetero- or euchromatin, for example) or cytoplasmic organelles such as the mitochondria networks. To ensure the best targeting accuracy, special care must be observed during the mounting of the culture dishes to avoid any unwanted source of optical distortion.

Several radiation biology experiments and developments are planned using the MIRCOM microbeam. For example, the characterization of the relationship between energy deposition at the nanometric scale and the initial biological events, initiated in the framework of the BioQuaRT project [60], will continue, to provide additional reference data points to improve the success and reliability of Monte Carlo track structure simulation codes. The development of ultra-thin microfluidic chips will be carried out to allow the irradiation of additional biological samples such as circulating cell types, and small organisms (nematodes, fish embryos, etc.). Following this, the biological consequences of mitochondrial irradiation will be studied, at the molecular, cellular and multicellular scale on cells and in the nematode *Caenorhabditis elegans*.

6. Conclusion

We report here the development and commissioning of IRSN's new ion microbeam, specifically dedicated to targeted micro-irradiation of living biological samples.

MIRCOM is a fully operational microbeam facility, open to external users, able to provide different focused ion beams, from proton to oxygen or heavier ions, with energies ranging from 0.5 to 12 MeV, and LETs from 10 to 1250 keV·µm^{-1}. Its beam spot size and targeting accuracy have been measured on track detector and on living cells for 4 MeV protons. These performances are comparable to those of similar existing focused microbeams. The good beam stability over time, in addition with a regular beam monitoring, makes possible to control the number of ions sent on target by selecting an appropriate beam opening time, with a good relative uncertainty for mean numbers of ions per target of 100 or higher. With the development of thin ion detectors, placed on the path of the beam, irradiation of samples with a lower number of ions, down to 1 ion per target, will be available with a very small relative uncertainty.

The facility allows an accurate, reliable and reproducible targeting of micrometric structures of biological samples, either nuclear/sub-nuclear elements (hetero- or euchromatin, for example) or cytoplasmic organelles such as the mitochondria networks. Samples can be observed immediately after irradiation using online time-lapse imaging, to study fast radiation-induced mechanisms. In addition to the microbeam itself, the facility is equipped with a state of the art biology laboratory, specifically designed to prepare biological samples for microbeam irradiation. Its location in close proximity to the microbeam room allows to quickly perform offline post-irradiation analysis.

Future developments such as the use of heavier ions and the implementation of microfluidic systems will improve further the versatility of the facility, making it possible to irradiate a wide variety of biological samples, from cellular to multicellular organisms.

Acknowledgements

The authors would like to thank P. Barberet (CENBG, France) for his help and precious advice all along the commissioning of the beamline, H. Seznec (CENBG, France) for his help in the sample preparation protocols, P. Alfaurt, M. Roche, and J. Outrequin (CENBG, France) for their work in developing the microbeam line, and for their precious help in the setting-up and commissioning of the beamline.

References

[1] R.E. Zirkle, W. Bloom, Irradiation of parts of individual cells., Science. 117 (1953) 487–93. https://doi.org/10.1126/science.117.3045.487.

[2] M. Ghita, C. Fernandez-Palomo, H. Fukunaga, P.M. Fredericia, G. Schettino, E. Bräuer-Krisch, K.T. Butterworth, S.J. McMahon, K.M. Prise, Microbeam evolution: from single cell irradiation to pre-clinical studies, Int. J. Radiat. Biol. 94 (2018) 708–718. https://doi.org/10.1080/09553002.2018.1425807.

[3] T.K. Hei, L.-J. Wu, S.-X. Liu, D. Vannais, C.A. Waldren, G. Randers-Pehrson, Mutagenic effects of a single and an exact number of particles in mammalian cells, Proc. Natl. Acad. Sci. 94 (1997) 3765–3770. https://doi.org/10.1073/pnas.94.8.3765.

[4] K.M. Prise, M. Folkard, A.M. Malcolmson, C.H.L. Pullar, G. Schettino, A.G. Bowey, B.D. Michael, Single ion actions: The induction of micronuclei in V79 cells exposed to individual protons, Adv. Sp. Res. 25 (2000) 2095–2101. https://doi.org/10.1016/S0273-1177(99)01060-1.

[5] B. Marples, M.C. Joiner, The response of Chinese hamster V79 cells to low radiation doses:

evidence of enhanced sensitivity of the whole cell population., Radiat. Res. 133 (1993) 41–51. http://www.ncbi.nlm.nih.gov/pubmed/8434112.

[6] C. Shao, Y. Furusawa, Y. Kobayashi, T. Funayama, S. Wada, Bystander effect induced by counted high-LET particles in confluent human fibroblasts: a mechanistic study, FASEB J. 17 (2003) 1422–1427. https://doi.org/10.1096/fj.02-1115com.

[7] N. Hamada, M. Ni, T. Funayama, T. Sakashita, Y. Kobayashi, Temporally distinct response of irradiated normal human fibroblasts and their bystander cells to energetic heavy ions, Mutat. Res. Mol. Mech. Mutagen. 639 (2008) 35–44. https://doi.org/10.1016/j.mrfmmm.2007.11.001.

[8] K. Harada, T. Nonaka, N. Hamada, H. Sakurai, M. Hasegawa, T. Funayama, T. Kakizaki, Y. Kobayashi, T. Nakano, Heavy-ion-induced bystander killing of human lung cancer cells: Role of gap junctional intercellular communication, Cancer Sci. 100 (2009) 684–688. https://doi.org/10.1111/j.1349-7006.2009.01093.x.

[9] K.M. Prise, G. Schettino, M. Folkard, K.D. Held, New insights on cell death from radiation exposure, Lancet Oncol. 6 (2005) 520–528. https://doi.org/10.1016/S1470-2045(05)70246-1.

[10] M.A. Kadhim, S.A. Lorimore, K.M.S. Townsend, D.T. Goodhead, V.J. Buckle, E.G. Wright, Radiation-induced Genomic Instability: Delayed Cytogenetic Aberrations and Apoptosis in Primary Human Bone Marrow Cells, Int. J. Radiat. Biol. 67 (1995) 287–293. https://doi.org/10.1080/09553009514550341.

[11] M.A. Kadhim, S.J. Marsden, D.T. Goodhead, A.M. Malcolmson, M. Folkard, K.M. Prise, B.D. Michael, Long-term genomic instability in human lymphocytes induced by single-particle irradiation., Radiat. Res. 155 (2001) 122–6. https://doi.org/10.1667/0033-7587(2001)155[0122:ltgiih]2.0.co;2.

[12] J.-B. Gorin, J. Ménager, S. Gouard, C. Maurel, Y. Guilloux, A. Faivre-Chauvet, A. Morgenstern, F. Bruchertseifer, M. Chérel, F. Davodeau, J. Gaschet, Antitumor Immunity Induced after α Irradiation, Neoplasia. 16 (2014) 319–328. https://doi.org/10.1016/j.neo.2014.04.002.

[13] G. Schettino, S.T. Al Rashid, K.M. Prise, Radiation microbeams as spatial and temporal probes of subcellular and tissue response, Mutat. Res. Mutat. Res. 704 (2010) 68–77. https://doi.org/10.1016/j.mrrev.2010.01.005.

[14] D.W.M. Walsh, C. Siebenwirth, C. Greubel, K. Ilicic, J. Reindl, S. Girst, G. Muggiolu, M. Simon, P. Barberet, H. Seznec, H. Zischka, G. Multhoff, T.E. Schmid, G. Dollinger, Live cell imaging of mitochondria following targeted irradiation in situ reveals rapid and highly localized loss of membrane potential, Sci. Rep. 7 (2017) 46684. https://doi.org/10.1038/srep46684.

[15] L. Tartier, S. Gilchrist, S. Burdak-Rothkamm, M. Folkard, K.M. Prise, Cytoplasmic Irradiation Induces Mitochondrial-Dependent 53BP1 Protein Relocalization in Irradiated and Bystander Cells, Cancer Res. 67 (2007) 5872–5879. https://doi.org/10.1158/0008-5472.CAN-07-0188.

[16] L.-J. Wu, G. Randers-Pehrson, A. Xu, C.A. Waldren, C.R. Geard, Z. Yu, T.K. Hei, Targeted cytoplasmic irradiation with alpha particles induces mutations in mammalian cells, Proc. Natl. Acad. Sci. 96 (1999) 4959–4964. https://doi.org/10.1073/pnas.96.9.4959.

[17] B. Zhang, M.M. Davidson, T.K. Hei, Mitochondria regulate DNA damage and genomic instability induced by high LET radiation, Life Sci. Sp. Res. 1 (2014) 80–88. https://doi.org/10.1016/j.lssr.2014.02.006.

[18] O. a Sedelnikova, A. Nakamura, O. Kovalchuk, I. Koturbash, S. a Mitchell, S. a Marino, D.J. Brenner, W.M. Bonner, DNA Double-Strand Breaks Form in Bystander Cells after Microbeam Irradiation of Three-dimensional Human Tissue Models, Cancer Res. 67 (2007) 4295–4302.

https://doi.org/10.1158/0008-5472.CAN-06-4442.

[19] M. Buonanno, G. Randers-Pehrson, L.B. Smilenov, N.J. Kleiman, E. Young, B. Ponnayia, D.J. Brenner, A Mouse Ear Model for Bystander Studies Induced by Microbeam Irradiation, Radiat. Res. 184 (2015) 219–225. https://doi.org/10.1667/RR14057.1.

[20] M. Suzuki, T. Sakashita, Y. Hattori, Y. Yokota, Y. Kobayashi, T. Funayama, Development of ultra-thin chips for immobilization of Caenorhabditis elegans in microfluidic channels during irradiation and selection of buffer solution to prevent dehydration, J. Neurosci. Methods. 306 (2018) 32–37. https://doi.org/10.1016/j.jneumeth.2018.05.025.

[21] T. Sakashita, T. Takanami, S. Yanase, N. Hamada, M. Suzuki, T. Kimura, Y. Kobayashi, N. Ishii, A. Higashitani, Radiation biology of Caenorhabditis elegans: germ cell response, aging and behavior., J. Radiat. Res. 51 (2010) 107–21. https://doi.org/10.1269/jrr.09100.

[22] K. Fukamoto, K. Shirai, T. Sakata, T. Sakashita, T. Funayama, N. Hamada, S. Wada, T. Kakizaki, S. Shimura, Y. Kobayashi, K. Kiguchi, Development of the irradiation method for the first instar silkworm larvae using locally targeted heavy-ion microbeam., J. Radiat. Res. 48 (2007) 247–53. https://doi.org/10.1269/jrr.06066.

[23] T. Yasuda, M. Kamahori, K. Nagata, T. Watanabe-Asaka, M. Suzuki, T. Funayama, H. Mitani, S. Oda, Abscopal Activation of Microglia in Embryonic Fish Brain Following Targeted Irradiation with Heavy-Ion Microbeam, Int. J. Mol. Sci. 18 (2017) 1428. https://doi.org/10.3390/ijms18071428.

[24] V. Gressier, G. Pelcot, J.L. Pochat, T. Bolognese-Milstajn, New IRSN facilities for neutron production, Nucl. Instruments Methods Phys. Res. Sect. A Accel. Spectrometers, Detect. Assoc. Equip. 505 (2003) 370–373. https://doi.org/10.1016/S0168-9002(03)01099-4.

[25] V. Gressier, J.F. Guerre-Chaley, V. Lacoste, L. Lebreton, G. Pelcot, J.L. Pochat, T. Bolognese-Milstajn, D. Champion, AMANDE: a new facility for monoenergetic neutron fields production between 2 keV and 20 MeV, Radiat. Prot. Dosimetry. 110 (2004) 49–52. https://doi.org/10.1093/rpd/nch185.

[26] G.W.W. Quax, A. Gottdang, D.J.W. Mous, A high-current light-ion injector for tandem accelerators, Rev. Sci. Instrum. 81 (2010) 02A701. https://doi.org/10.1063/1.3259235.

[27] M.G. Klein, D.J.W. Mous, A. Gottdang, A compact 1MV multi-element AMS system, Nucl. Instruments Methods Phys. Res. Sect. B Beam Interact. with Mater. Atoms. 249 (2006) 764–767. https://doi.org/10.1016/j.nimb.2006.03.135.

[28] M. Arnold, S. Merchel, D.L. Bourlès, R. Braucher, L. Benedetti, R.C. Finkel, G. Aumaître, A. Gottdang, M. Klein, The French accelerator mass spectrometry facility ASTER: Improved performance and developments, Nucl. Instruments Methods Phys. Res. Sect. B Beam Interact. with Mater. Atoms. 268 (2010) 1954–1959. https://doi.org/10.1016/j.nimb.2010.02.107.

[29] D.J.W. Mous, J. Visser, R.G. Haitsma, A nanosecond pulsing system for MeV light ions using a 2 MV TandetronTM, Nucl. Instruments Methods Phys. Res. Sect. B Beam Interact. with Mater. Atoms. 219–220 (2004) 490–493. https://doi.org/10.1016/j.nimb.2004.01.108.

[30] S.H. Sie, C.G. Ryan, D.R. Cousens, G.F. Suter, A Tandetron-based microbeam system, Nucl. Instruments Methods Phys. Res. Sect. B Beam Interact. with Mater. Atoms. 45 (1990) 543–547. https://doi.org/10.1016/0168-583X(90)90896-3.

[31] H. Imaseki, M. Yukawa, F. Watt, T. Ishikawa, H. Iso, T. Hamano, K. Matsumoto, N. Yasuda, The scanning microbeam PIXE analysis facility at NIRS, Nucl. Instruments Methods Phys. Res. Sect. B Beam Interact. with Mater. Atoms. 210 (2003) 42–47. https://doi.org/10.1016/S0168-

583X(03)01002-4.

[32] O. Enguita, M.T. Fernández-Jiménez, G. García, A. Climent-Font, T. Calderón, G.W. Grime, The new external microbeam facility at the 5 MV Tandetron accelerator laboratory in Madrid: beam characterisation and first results, Nucl. Instruments Methods Phys. Res. Sect. B Beam Interact. with Mater. Atoms. 219–220 (2004) 384–388. https://doi.org/10.1016/j.nimb.2004.01.087.

[33] M. Jakšić, I. Bogdanović Radović, M. Bogovac, V. Desnica, S. Fazinić, M. Karlušić, Z. Medunić, H. Muto, Ž. Pastuović, Z. Siketić, N. Skukan, T. Tadić, New capabilities of the Zagreb ion microbeam system, Nucl. Instruments Methods Phys. Res. Sect. B Beam Interact. with Mater. Atoms. 260 (2007) 114–118. https://doi.org/10.1016/j.nimb.2007.01.252.

[34] M.J. Merchant, J.C.G. Jeynes, G.W. Grime, V. Palitsin, I.D.W. Tullis, P.R. Barber, B. Vojnovic, R.P. Webb, K.J. Kirkby, A Focused Scanning Vertical Beam for Charged Particle Irradiation of Living Cells with Single Counted Particles, Radiat. Res. 178 (2012) 182–190. https://doi.org/10.1667/RR2847.1.

[35] I. Burducea, M. Straticiuc, D.G. Ghiță, D.V. Moșu, C.I. Călinescu, N.C. Podaru, D.J.W. Mous, I. Ursu, N.V. Zamfir, A new ion beam facility based on a 3 MV Tandetron™ at IFIN-HH, Romania, Nucl. Instruments Methods Phys. Res. Sect. B Beam Interact. with Mater. Atoms. 359 (2015) 12–19. https://doi.org/10.1016/j.nimb.2015.07.011.

[36] S. Bourret, F. Vianna, G. Devès, V. Atallah, P. Moretto, H. Seznec, P. Barberet, Fluorescence time-lapse imaging of single cells targeted with a focused scanning charged-particle microbeam, Nucl. Instruments Methods Phys. Res. Sect. B Beam Interact. with Mater. Atoms. 325 (2014) 27–34. https://doi.org/10.1016/j.nimb.2014.02.004.

[37] S. Incerti, Q. Zhang, F. Andersson, P. Moretto, G.W. Grime, M.J. Merchant, D.T. Nguyen, C. Habchi, T. Pouthier, H. Seznec, Monte Carlo simulation of the CENBG microbeam and nanobeam lines with the Geant4 toolkit, Nucl. Instruments Methods Phys. Res. Sect. B Beam Interact. with Mater. Atoms. 260 (2007) 20–27. https://doi.org/10.1016/j.nimb.2007.01.274.

[38] L. Daudin, P. Barberet, L. Serani, P. Moretto, CRionScan: A stand-alone real time controller designed to perform ion beam imaging, dose controlled irradiation and proton beam writing, Nucl. Instruments Methods Phys. Res. Sect. B Beam Interact. with Mater. Atoms. 306 (2013) 64–70. https://doi.org/10.1016/j.nimb.2012.11.041.

[39] J.F. Ziegler, M.D. Ziegler, J.P. Biersack, SRIM – The stopping and range of ions in matter (2010), Nucl. Instruments Methods Phys. Res. Sect. B Beam Interact. with Mater. Atoms. 268 (2010) 1818–1823. https://doi.org/10.1016/j.nimb.2010.02.091.

[40] S. Agostinelli, J. Allison, K. Amako, J. Apostolakis, H. Araujo, P. Arce, M. Asai, D. Axen, S. Banerjee, G. Barrand, F. Behner, L. Bellagamba, J. Boudreau, L. Broglia, A. Brunengo, H. Burkhardt, S. Chauvie, J. Chuma, R. Chytracek, G. Cooperman, G. Cosmo, P. Degtyarenko, A. Dell'Acqua, G. Depaola, D. Dietrich, R. Enami, A. Feliciello, C. Ferguson, H. Fesefeldt, G. Folger, F. Foppiano, A. Forti, S. Garelli, S. Giani, R. Giannitrapani, D. Gibin, J.J. Gómez Cadenas, I. González, G. Gracia Abril, G. Greeniaus, W. Greiner, V. Grichine, A. Grossheim, S. Guatelli, P. Gumplinger, R. Hamatsu, K. Hashimoto, H. Hasui, A. Heikkinen, A. Howard, V. Ivanchenko, A. Johnson, F.W. Jones, J. Kallenbach, N. Kanaya, M. Kawabata, Y. Kawabata, M. Kawaguti, S. Kelner, P. Kent, A. Kimura, T. Kodama, R. Kokoulin, M. Kossov, H. Kurashige, E. Lamanna, T. Lampén, V. Lara, V. Lefebure, F. Lei, M. Liendl, W. Lockman, F. Longo, S. Magni, M. Maire, E. Medernach, K. Minamimoto, P. Mora de Freitas, Y. Morita, K. Murakami, M. Nagamatu, R. Nartallo, P. Nieminen, T. Nishimura, K. Ohtsubo, M. Okamura, S. O'Neale, Y. Oohata, K. Paech, J. Perl, A. Pfeiffer, M.G. Pia, F. Ranjard, A. Rybin, S. Sadilov, E. Di Salvo, G. Santin, T. Sasaki, N. Savvas, Y. Sawada, S. Scherer, S. Sei, V. Sirotenko, D. Smith, N. Starkov, H. Stoecker, J. Sulkimo,

M. Takahata, S. Tanaka, E. Tcherniaev, E. Safai Tehrani, M. Tropeano, P. Truscott, H. Uno, L. Urban, P. Urban, M. Verderi, A. Walkden, W. Wander, H. Weber, J.P. Wellisch, T. Wenaus, D.C. Williams, D. Wright, T. Yamada, H. Yoshida, D. Zschiesche, Geant4—a simulation toolkit, Nucl. Instruments Methods Phys. Res. Sect. A Accel. Spectrometers, Detect. Assoc. Equip. 506 (2003) 250–303. https://doi.org/10.1016/S0168-9002(03)01368-8.

[41] S. Peng, M. Folkard, S. Gilchrist, R.J. Locke, Z. Yu, B.D. Michael, Measurements of the targeting accuracy of the Gray Laboratory charged-particle microbeam, Nucl. Instruments Methods Phys. Res. Sect. B Beam Interact. with Mater. Atoms. 179 (2001) 145–150. https://doi.org/10.1016/S0168-583X(01)00388-3.

[42] M. Heiß, B.E. Fischer, B. Jakob, C. Fournier, G. Becker, G. Taucher-Scholz, Targeted Irradiation of Mammalian Cells Using a Heavy-Ion Microprobe, Radiat. Res. 165 (2006) 231–239. https://doi.org/10.1667/RR3495.1.

[43] T. Funayama, S. Wada, Y. Yokota, K. Fukamoto, T. Sakashita, M. Taguchi, T. Kakizaki, N. Hamada, M. Suzuki, Y. Furusawa, H. Watanabe, K. Kiguchi, Y. Kobayashi, Heavy-ion microbeam system at JAEA-Takasaki for microbeam biology., J. Radiat. Res. 49 (2008) 71–82. https://doi.org/10.1269/jrr.07085.

[44] K. Greif, W. Beverung, F. Langner, D. Frankenberg, A. Gellhaus, F. Banaz-Yasar, The PTB microbeam: a versatile instrument for radiobiological research, Radiat. Prot. Dosimetry. 122 (2006) 313–315. https://doi.org/10.1093/rpd/ncl436.

[45] B. Jakob, J.H. Rudolph, N. Gueven, M.F. Lavin, G. Taucher-Scholz, Live Cell Imaging of Heavy-Ion-Induced Radiation Responses by Beamline Microscopy, Radiat. Res. 163 (2005) 681–690. https://doi.org/10.1667/RR3374.

[46] K.H. Almeida, R.W. Sobol, A unified view of base excision repair: Lesion-dependent protein complexes regulated by post-translational modification, DNA Repair (Amst). 6 (2007) 695–711. https://doi.org/10.1016/j.dnarep.2007.01.009.

[47] K.W. Caldecott, Single-strand break repair and genetic disease., Nat. Rev. Genet. 9 (2008) 619–31. https://doi.org/10.1038/nrg2380.

[48] T. Ogi, S. Limsirichaikul, R.M. Overmeer, M. Volker, K. Takenaka, R. Cloney, Y. Nakazawa, A. Niimi, Y. Miki, N.G. Jaspers, L.H.F. Mullenders, S. Yamashita, M.I. Fousteri, A.R. Lehmann, Three DNA Polymerases, Recruited by Different Mechanisms, Carry Out NER Repair Synthesis in Human Cells, Mol. Cell. 37 (2010) 714–727. https://doi.org/10.1016/j.molcel.2010.02.009.

[49] T.W. Kirby, N.R. Gassman, C.E. Smith, L.C. Pedersen, S.A. Gabel, M. Sobhany, S.H. Wilson, R.E. London, Nuclear Localization of the DNA Repair Scaffold XRCC1: Uncovering the Functional Role of a Bipartite NLS, Sci. Rep. 5 (2015) 13405. https://doi.org/10.1038/srep13405.

[50] O. Mortusewicz, H. Leonhardt, XRCC1 and PCNA are loading platforms with distinct kinetic properties and different capacities to respond to multiple DNA lesions, BMC Mol. Biol. 8 (2007) 81. https://doi.org/10.1186/1471-2199-8-81.

[51] J. Schindelin, I. Arganda-Carreras, E. Frise, V. Kaynig, M. Longair, T. Pietzsch, S. Preibisch, C. Rueden, S. Saalfeld, B. Schmid, J. Tinevez, D.J. White, V. Hartenstein, K. Eliceiri, P. Tomancak, A. Cardona, Fiji: an open-source platform for biological-image analysis, Nat. Methods. 9 (2012) 676–682. https://doi.org/10.1038/nmeth.2019.

[52] P. Barberet, M. Pomorski, G. Muggiolu, E. Torfeh, G. Claverie, C. Huss, S. Saada, G. Devès, M. Simon, H. Seznec, Cell micro-irradiation with MeV protons counted by an ultra-thin diamond membrane, Appl. Phys. Lett. 111 (2017) 243701. https://doi.org/10.1063/1.5009713.

[53] B.E. Fischer, M. Heiß, M. Cholewa, About the art to shoot with single ions, Nucl. Instruments Methods Phys. Res. Sect. B Beam Interact. with Mater. Atoms. 210 (2003) 285–291. https://doi.org/10.1016/S0168-583X(03)01038-3.

[54] T. Konishi, M. Oikawa, N. Suya, T. Ishikawa, T. Maeda, A. Kobayashi, N. Shiomi, K. Kodama, T. Hamano, S. Homma-Takeda, M. Isono, K. Hieda, Y. Uchihori, Y. Shirakawa, SPICE-NIRS Microbeam: a focused vertical system for proton irradiation of a single cell for radiobiological research, J. Radiat. Res. 54 (2013) 736–747. https://doi.org/10.1093/jrr/rrs132.

[55] X.F. Wang, J.Q. Li, J.Z. Wang, J.X. Zhang, A. Liu, Z.J. He, W. Zhang, B. Zhang, C.L. Shao, L.Q. Shi, Current progress of the biological single-ion microbeam at FUDAN, Radiat. Environ. Biophys. 50 (2011) 353–364. https://doi.org/10.1007/s00411-011-0361-1.

[56] M. Mosconi, U. Giesen, F. Langner, C. Mielke, I. Dalla Rosa, W.G. Dirks, 53BP1 and MDC1 foci formation in HT-1080 cells for low- and high-LET microbeam irradiations, Radiat. Environ. Biophys. 50 (2011) 345–352. https://doi.org/10.1007/s00411-011-0366-9.

[57] S. Incerti, C. Habchi, P. Moretto, J. Olivier, H. Seznec, Geant4 simulation of the new CENBG micro and nanoprobes facility, Nucl. Instruments Methods Phys. Res. Sect. B Beam Interact. with Mater. Atoms. 249 (2006) 738–742. https://doi.org/10.1016/j.nimb.2006.03.130.

[58] E. Torfeh, M. Simon, G. Muggiolu, G. Devès, F. Vianna, S. Bourret, S. Incerti, P. Barberet, H. Seznec, Monte-Carlo dosimetry and real-time imaging of targeted irradiation consequences in 2-cell stage Caenorhabditis elegans embryo, Sci. Rep. 9 (2019) 10568. https://doi.org/10.1038/s41598-019-47122-7.

[59] S.B.C. Debnath, C. Fauquet, A. Tallet, A. Goncalves, S. Lavandier, F. Jandard, D. Tonneau, J. Darreon, High spatial resolution inorganic scintillator detector for high-energy X-ray beam at small field irradiation, Med. Phys. 47 (2020) 1364–1371. https://doi.org/10.1002/mp.14002.

[60] G. Gonon, C. Villagrasa, P. Voisin, S. Meylan, M. Bueno, M.A. Benadjaoud, N. Tang, F. Langner, H. Rabus, J.-F. Barquinero, U. Giesen, G. Gruel, From Energy Deposition of Ionizing Radiation to Cell Damage Signaling: Benchmarking Simulations by Measured Yields of Initial DNA Damage after Ion Microbeam Irradiation, Radiat. Res. 191 (2019) 566. https://doi.org/10.1667/RR15312.1.